

Divergent Paradigms of Porphyry Cu Deposits in Subduction and Collision Zones

Zixuan Wang¹, Yuanchuan Zheng^{1*}, Massimo Chiaradia²,
Bo Xu¹, Hongda Hao³, Zengqian Hou³

^{1*}State Key Laboratory of Geological Processes and Mineral Resources,
Frontiers Science Center for Deep-Time Digital Earth, China University
of Geosciences, Beijing, 100083, China.

²Department of Earth Sciences, University of Geneva, Geneva, 1205,
Switzerland.

³Institute of Geology, Chinese Academy of Geological Sciences, Beijing,
100037, China.

*Corresponding author(s). E-mail(s): zheng_yc@126.com;
Contributing authors: wangzx@cugb.edu.cn;
massimo.chiaradia@unige.ch; bo.xu@cugb.edu.cn;
hongda.hao@hotmail.com; houzengqian@126.com;

Abstract

The prevailing view suggests that the formation of porphyry Cu deposits involves differentiation of water-rich, metal-bearing juvenile magmas, with subduction of oceanic slabs supplying the necessary volatiles. However, the occurrence of significant porphyry Cu deposits in continental collision zones, where such volatile sources are absent, challenges this paradigm. We analyze a global dataset of whole-rock platinum-group elements and apatite compositions of ore-forming magmas in both subduction and collision zones, combined with Monte Carlo simulations. The results reveal that ore-forming magmas in collision zones exhibit significantly higher degassing efficiencies compared to those in subduction zones. To explain this, we integrate whole-rock geochemistry, mineral thermobarometry, and thermodynamic modeling, proposing that lower water contents of collision zone ore-forming magmas lead to shallower magma storage depths, significantly enhancing degassing efficiency. In contrast, higher water contents of subduction zone ore-forming magmas result in greater emplacements, limiting degassing efficiency. Despite this limitation, larger magma volumes in subduction zones compensate for lower degassing efficiencies. These findings highlight distinct

frameworks of water content, storage depth, and magma volume between subduction and collision zone porphyry Cu deposits. The synergistic interplay of these factors is fundamental to porphyry Cu formation.

1 Introduction

The characteristics and cycling of volatiles on Earth differ significantly from those on other planets in our Solar System, playing a critical role in sustaining life, regulating Earth’s climate, and producing resources that are indispensable to society [1]. As a key carrier of volatiles, magmas can transport volatiles from depth to the shallow crust, where they undergo degassing processes, forming hot springs, triggering explosive volcanism, or generating economically valuable porphyry Cu deposits (PCDs) [2].

Traditionally, water-rich magmas, enriched in volatiles, are fundamental to the formation of PCDs [2, 3]. In subduction zones, oceanic slabs release large amounts of volatiles during subduction, which metasomatize the overlying mantle wedge, causing partial melting and forming water-rich, metal-bearing juvenile magmas [4, 5]. As these magmas ascend, differentiate, and degas, they ultimately provide the metal-rich magmatic fluids for the formation of PCDs [6]. Recent studies have shown that volatiles released during the subduction of oceanic plates not only affect the overlying mantle but can also directly cause partial melting of the lower crust during flat-slab subduction, forming metal-bearing juvenile magmas [7]. Thus, the volatiles released from subducting oceanic slabs are regarded as playing a crucial role in PCD mineralization.

Continental collision zones, another important component of convergent plate boundaries, also host a significant number of PCDs, constituting important PCD metallogenic belts [6, 8]. However, collision zones lack direct volatile supply from subducting oceanic slabs, resulting in relatively dry juvenile magmas compared to those in subduction zones. The smaller volumes of volcanic rocks formed in collision zones, relative to subduction zones, support the idea that juvenile magmas in collision zones are relatively water-poor (Extended Data Fig. 1), as fluid-driven flux melting in subduction zones tends to generate larger magma volumes [9]. The existence of PCDs in collision zones challenges the traditional view that high water content magmas, controlled by volatiles released from subducting slabs, are essential for PCD mineralization. Instead, the formation of PCDs is governed by complex frameworks involving magma water content, volume, emplacement depth, and degassing processes [5, 6, 10]. Therefore, a systematic comparison of subduction and collision zone PCDs is critical to identifying the key mechanisms controlling PCD formation.

Here we compare the degassing efficiencies and the frameworks controlling PCD mineralisation in subduction and collision zones, by taking advantage of increased availability of whole-rock major-element, platinum-group elements (PGEs), apatite composition data, combined with mineral thermobarometry, thermodynamic modeling, and Monte Carlo simulations. We posit that this comparison provides insight not

only on the synergistic frameworks required for PCD formation, but also on the cycling mechanisms of volatiles at convergent plate boundaries.

2 Dataset of Ore-Forming Magmatic Characteristics in Subduction and Collision Zones

Convergent plate boundaries are broadly classified into subduction and collision zones. Subduction zones are defined by the subduction of oceanic slabs, typically associated with arc magmatism and the formation of accretionary orogens. In contrast, collision zones primarily result from continental plate collisions, leading to lithospheric thickening, the development of collisional orogens, and associated magmatism [11, 12]. This collision-related magmatism often occurs after a significant temporal gap following earlier arc magmatism [8, 13]. By the time collisional orogeny initiates, the subducted oceanic slab has already undergone detachment or rollback, marking a fundamental transition in tectonic processes. Consequently, the tectonic settings of PCDs in subduction and collision zones differ markedly, primarily due to the presence or absence of a subducting oceanic slab [8, 11].

Traditionally, the source region for ore-forming magmas in subduction zones has been attributed to the mantle wedge above the subducting slab [4, 5]. However, recent research suggests that in regions with flat-slab subduction, the source region may also reside in the lower crust [7]. In either case, the subduction of oceanic slabs release substantial volatile components, promoting fluid-driven flux melting in the source region and generating the water-rich, juvenile magmas necessary for PCD formation [5, 14, 15]. By contrast, the source regions of ore-forming magmas in collision zones are generally located within the lithosphere (lower crust or lithospheric mantle) [8, 16, 17], and the mechanisms of partial melting remain debated, with proposed models including asthenospheric upwelling and lithospheric delamination [18, 19]. The absence of subducting oceanic slabs in collision zones results in magma genesis mechanisms distinct from fluid-driven flux melting, leading to notable geochemical differences between ore-forming magmas in these two tectonic settings. Subduction-related magmas are typically intermediate calc-alkaline series, whereas collision-related magmas are more felsic and alkali-rich [20, 21].

To systematically compare the magmatic-mineralization features of PCDs in subduction and collision zones, we compiled a global dataset comprising whole-rock geochemical data for major elements, PGEs, and mineral compositions (apatite, amphibole, and zircon) from 44 PCDs (Supplementary Table S1–4). Of these, 24 deposits are from subduction zones and 20 from collision zones, encompassing major convergent plate boundaries worldwide to ensure the data’s broad applicability (Fig. 1). While not all PCDs provide complete geochemical and mineralogical datasets, we maximized the information gathered and ensured a balance between subduction and collision zones to minimize bias arising from unequal sample sizes. Recognizing that multiple magmatic events often occur within a single PCD, we excluded samples unrelated to PCD mineralization, ensuring that the selected data reflect the geochemical and mineralogical characteristics of ore-forming magmas.

This study classifies PCDs based on their tectonic settings (subduction vs. collision zones), a classification scheme that complements traditional categorizations into syn-subduction and post-subduction PCDs. The post-subduction stage may encompass multiple phases, including pre-collision, syn-collision, and post-collision processes. However, our focus is to examine the potential influence of oceanic slab subduction on metallogenesis. Although post-subduction PCDs are commonly associated with the cessation of oceanic slab subduction, the possibility of continued slab-derived material supply remains [22]. To ensure a clear distinction between subduction and collision zone PCDs, we excluded deposits with debated tectonic environments (e.g., Grasberg) to maintain a robust comparative framework for evaluating metallogenic mechanisms.

3 Identifying the Degassing Processes of Ore-Forming Magmas

Compared to collision zones, ore-forming magmas in subduction zones generally have lower SiO_2 and higher MgO contents (Extended Data Fig. 2). This difference may arise from variations in both parental magma composition and subsequent magmatic evolution. Specifically, the source region in subduction zones is likely a more mafic mantle wedge, where fluid-driven flux melting generates high-MgO parental magmas. The samples with the highest MgO content in subduction zone ore-forming magmas have PGE concentrations comparable to those of primitive arc magma ($\text{Pd} \approx 1$ to 7 ppb and $\text{Pt} \approx 1.5$ to 5 ppb) [23]. In contrast, ore-forming magmas in collision zones, derived from a thickened lithosphere, typically exhibit lower MgO content and correspondingly lower initial PGE concentrations (Fig. 2a, b). Moreover, magmatic differentiation influences the final magma compositions in both settings, but the distinct source processes dictate the initial magma characteristics and influence their subsequent evolution.

PGEs are typically incompatible with silicate and oxide minerals, but strongly compatible with sulfide melts [24, 25]. The rapid decrease in Pd abundance observed in both subduction and collision zone ore-forming magmas with < 3 wt% MgO suggests that sulfide segregation occurs during the late stages of magma evolution for ore-forming magmas in both tectonic settings (Fig. 2a). Late sulfide segregation prevents metal to be sequestered by early magmatic sulfides, allowing them to be extracted by fluids and precipitated in the PCD mineralization [24, 25]. Additionally, some samples from the Escondida deposit in the subduction zone and the Qulong and Dalli deposits in the collision zone show lower Pd concentrations at > 3 wt% MgO (Fig. 2a, b; Extended Data Fig. 3a, c), suggesting that sulfide segregation occurred at an earlier stage of magma evolution. Some models advocate the need of Cu-rich magmas for PCD formation, arguing that early sulfide segregation depletes metals, thereby reducing magma fertility [24–26]. However, other models propose that PCDs can also form from magmas with normal metal contents, with factors such as magmatic evolution, sulfide recycling, and the concentration of ore-forming components through magma degassing playing key roles [27–29]. Both the Escondida and Qulong deposits are giant PCDs, indicating that their early-stage sulfide saturation did not prevent significant mineralization. The interplay between melt evolution, sulfide segregation, and magma

degassing, along with their combined effects on metal distribution, plays a more critical role.

There are differences in the compatibility of PGEs in sulfides, with Pd being more compatible than Pt. This suggests that if only sulfide segregation occurs in the magma system, more Pd would be consumed, resulting in a decrease in the Pd/Pt ratios [25, 30]. However, both subduction and collision zone ore-forming magmas show an increasing trend in Pd/Pt ratios as MgO contents decrease below 3 wt% (Fig. 2c, d). Moreover, in the Escondida, Qulong, and Dalli deposits, samples with > 3 wt% MgO exhibit lower Pd concentrations but Pd/Pt ratios greater than ~ 1 (Extended Data Fig. 3). This is inconsistent with the characteristic behavior of sulfide segregation alone and suggests the presence of other Pt consumption processes. One possible explanation is the segregation of Pt-rich alloys, which could consume Pt, causing the Pd/Pt ratios to rise [31]. However, as magmas evolve, the decreasing trend in Pd abundance suggests that sulfide segregation occurs below 3 wt% MgO. This process strongly consumes Pt, preventing the saturation of Pt-rich alloys [31], thereby dismissing the hypothesis that the segregation of Pt-rich alloys leads to an increase in Pd/Pt ratios.

Although the compatibility of PGEs in fluids is much lower than that in sulfides, the volume of fluid generated during the degassing of shallow magma significantly exceeds the amount of segregated sulfides, necessitating a reassessment of the impact of fluids on PGE concentrations. Furthermore, the compatibility of PGEs in fluids differ markedly, with Pt being more compatible than Pd [30], indicating that the degassing processes may lead to an increase in Pd/Pt ratios. To explore this, we employed a Monte Carlo method to simulate the evolution of PGE compositions during magma differentiation and degassing, and compared the results with the PGE characteristics of ore-forming magmas in subduction and collision zones (Fig. 2; Methods). The results show that the rapid decrease in Pd contents, which occurs as MgO contents fall below 3 wt%, indeed indicates sulfide segregation (Fig. 2a). However, the amount of metals removed by sulfide segregation may be limited, with a considerable proportion of metals potentially partitioned into the exsolved fluid phase (Fig. 2b).

The model results for the Pd/Pt ratio suggest that, owing to variations in initial water contents and magma evolution processes, the timing of fluid saturation can differ significantly. When MgO content is < 3 wt%, the Pd/Pt ratios in both subduction and collision zone ore-forming magmas increases markedly, closely aligning with the regions in the models where fluid saturation occurs and carries significant amounts of metals (Fig. 2d). This suggests that the degassing processes in both subduction and collision zone ore-forming magmas play a significant role in redistributing large amounts of metals. Additionally, the presence of more samples in the subduction zones with higher MgO content, or lower MgO content but with low Pd/Pt ratios ($< \sim 1$; Extended Data Fig. 3a, b), indicates a relatively lower proportion of metals carried by the fluid (Fig. 2d). The PGE characteristics suggest that ore-forming magmas in both subduction and collision zones have undergone degassing, which is essential for PCD mineralization [5, 6, 10, 20]. The differences in the proportion of metals carried by fluids further imply that the degassing efficiency of ore-forming magmas varies between subduction and collision zones.

4 Distinct Degassing Efficiency between Subduction and Collision Zone PCDs

Apatite, a volatile-rich mineral, is an ideal proxy for constraining the evolution of magma volatiles [32–34]. As shown in Extended Data Fig. 4 and 5, there are significant compositional differences between apatites from subduction and collision zones. Apatites from subduction zone ore-forming magmas are more enriched in Cl, whereas those from collision zone ore-forming magmas are more enriched in F. Using the compositions of apatite and the temperatures of apatite saturation (AST) calculated from whole-rock major elements, we can determine the absolute concentrations of Cl, F, and OH in the melt, as well as the volatile ratios (F/Cl; F/OH; Cl/OH; Methods) [35]. The melt volatile ratios in subduction zone ore-forming magmas differ markedly from those in collision zones, with subduction zone melts exhibiting notably lower Melt X_F/X_{Cl} ratios but higher Melt X_{Cl}/X_{OH} ratios compared to collision zone melts (Fig. 3). These differences clearly separate subduction and collision zone ore-forming melts into two distinct groups. However, whether these characteristics reflect initial volatile composition differences or variations in magma evolution and degassing processes remains uncertain.

Monte Carlo simulations were performed to show melt volatile evolution and a comparison with melt compositions inferred from individual apatite compositions. Parameters are randomly selected from pre-defined, realistic ranges, which allows the models to account for the large uncertainty in starting conditions (Methods) [36]. The results show that the volatile compositions of most subduction zone ore-forming magmas and nearly all collision zone ore-forming magmas align with the fluid-saturated model results (Fig. 3a, b). However, a subset of subduction zone ore-forming magmas exhibits melt characteristics indicative of fluid-undersaturated conditions (Fig. 3c, d). Even under broad starting volatile compositions, the simulated initial volatile ratios remain relatively concentrated, failing to account for the substantial differences in volatile ratios between subduction and collision zone ore-forming magmas (Fig. 3).

We further constrained the degassing efficiencies at different stages of volatile evolution and found that subduction zone ore-forming magmas generally exhibit low degrees of fluid exsolution ($< \sim 40\%$), while collision zone ore-forming magmas typically show fluid exsolution exceeding 40%, and even reaching up to $\sim 80\%$ (Fig. 3a, b). This indicates that the degassing efficiencies of collision zone ore-forming magmas are significantly higher than those of subduction zone. For some subduction zone ore-forming magmas, melt volatile characteristics indicate the absence of fluid exsolution (Fig. 3c, d). This could be attributed to the apatites recording these melts failing to capture the fluid saturation processes, potentially suggesting that fluid saturation occurs at relatively late stages in subduction zones. This observation aligns with whole-rock major element and PGE compositional characteristics, which show that the juvenile ore-forming magmas in subduction zone typically have lower SiO_2 and higher MgO , requiring long evolutionary processes to achieve fluid saturation at $\text{MgO} < 3 \text{ wt}\%$ (Fig. 2b, d).

5 Magma Storage Depth Controls Degassing Efficiency

Determining the initial water content of magmas is challenging, especially for ore-forming magmas that have undergone significant differentiation, which obscures primary volatile signatures. Initial water content is controlled by multiple factors, including crustal thickness, source temperature, water content, and the degree of partial melting, resulting in considerable variability [37]. While both subduction and collision zones involve lithospheric thickening and may share similar melting conditions, subduction zone ore-forming magmas likely have higher initial water contents than those of collision zones, owing to the direct supply of volatiles from subducting oceanic slabs. If magmatic processes were similar, magmas with higher initial water contents would be expected to reach fluid saturation earlier, achieving higher degassing efficiencies. However, subduction zone ore-forming magmas exhibit lower degassing efficiencies compared to collision zone magmas, reflecting distinct magmatic processes in these two tectonic settings.

The process of fluid saturation is controlled not only by magma water contents but also by magma storage depths. As pressure decreases, the water solubility in magma progressively declines [38]. This implies that magmas stored in shallower magma chambers have lower water solubility, making them more prone to fluid saturation and facilitating higher degassing efficiencies during magma evolution. Both subduction and collision zone ore-forming magmas commonly contain amphibole phenocrysts, which can record information about processes occurring in shallow magma chambers [6, 39].

Amphibole barometry results indicate that the storage depths of ore-forming magmas in subduction zones are obviously greater than those in collision zones (Extended Data Fig. 6). Despite the uncertainties associated with amphibole barometry, particularly in the analysis of individual magmatic systems, the systematic differences observed between subduction and collision zone ore-forming magmas are unlikely to arise from methodological limitations. The results from both amphibole and zircon thermometry consistently show that subduction zone ore-forming magmas are generally hotter than those in collision zones (Extended Data Fig. 6). These temperature differences cannot be attributed to disparities in magma water content, as subduction zone magmas, which are likely more water-rich, should exhibit lower temperatures [40]. Therefore, the greater storage depths of subduction zone ore-forming magmas compared to those in collision zones provide a compelling explanation for the differences in their degassing efficiencies.

6 Synergistic Frameworks of Magmatic Properties, Structure, and Volume

Increasing evidences suggest that magma storage depth may correlate with water content of magmas [41–43]. During magma ascent, melt viscosity increases continuously as the water solubility progressively decreases, ultimately leading to fluid saturation and degassing [40, 43–45]. Degassing processes increase melt viscosity, inhibiting magma

ascent, while also promoting cooling and crystallization that further amplify melt viscosity. When the increase in melt viscosity reaches its maximum convexity (viscosity knee) during ascent, the magma halts its upward movement and forms a reservoir in the crust [43]. We conducted thermodynamic modeling using rhyolite-MELTS to simulate magma viscosity changes under both open- and closed-system during ascent, in order to examine the effects of different initial water contents (Methods).

The modeling results reveal that higher initial water contents shift the viscosity knee to greater depths, indicating deeper magma storage (Fig. 4), which is consistent with our findings [46]. The juvenile magmas of subduction zone PCDs, characterized by higher water contents, experience viscosity stalling at greater depths, forming magma reservoirs. These greater magma storage depths restrict fluid saturation, leading to lower degassing efficiencies. In contrast, the lower initial water contents of collision zone ore-forming magmas lead to the formation of shallower magma reservoirs, facilitating fluid saturation and higher degassing efficiencies. However, it is the total volume of ore-forming fluid released from the magma system that governs PCD mineralization. This total output is controlled by two key factors: degassing efficiency and magma volume [27, 47]. Therefore, two contrasting but equally viable mineralization processes must be considered: large magma volumes but lower degassing efficiencies versus smaller magma volumes but higher degassing efficiencies. Both processes can generate sufficient ore-forming fluids to form PCDs.

Subduction zone magmas form most of the world’s significant PCD metallogenic belts [48], which can be attributed to the larger magma volumes of ore-forming magmas in subduction zones. Although degassing efficiencies are lower, the large magma volumes compensate by generating sufficient ore-forming fluids to support PCD mineralization. Magma volume can be inferred from the probability of eruption, and global data show that subduction zones have significantly larger eruption volumes than collision zones (Extended Data Fig. 1). This indicates the larger volumes of ore-forming magmas in subduction zones. Such differences are consistent with contrasting processes that generate juvenile magmas, where fluid-driven flux melting in subduction zones is more efficient and produces larger magma volumes (Fig. 5) [15, 49], exhibiting long-lived, sustained magma supply [50]. These larger magma volumes compensate for lower degassing efficiencies, ultimately enabling the formation of PCDs. In contrast, although magma volumes are limited in collision zones due to the transient, episodic melting windows [50], higher degassing efficiencies ensure the availability of sufficient ore-forming fluids to generate PCD mineralization.

Although both subduction and collision zones generate significant PCDs and world-class PCD metallogenic belts, the ore-forming magmas exhibit substantial differences in magma volume, water content, storage depth, and degassing efficiency. These differences define distinct synergistic frameworks that ultimately control PCD mineralization. Our results also suggest significant differences in the cycling of volatiles between different convergent plate boundaries. In subduction zones, a considerable portion of the volatiles supplied by subducting oceanic slabs may be stored in the deeper lithosphere. However, larger magma volumes can still transport large volumes of volatiles to shallower depths and even release them directly to the Earth’s surface.

In contrast, lower magma volumes play a crucial role in volatile cycling through more efficient degassing processes in collision zones.

7 Methods

7.1 Data Acquisition for Ore-Forming Magmas in Subduction and Collision Zones

To uncover the differences between ore-forming magmas in subduction and collision zones, this study compiled and analyzed whole-rock major element compositions, PGE characteristics, and mineral compositional data (apatite, amphibole, and zircon) from 44 PCDs worldwide (Supplementary Table S1–4). Given the focus on contrasting ore-forming processes under different tectonic settings, we retained only data directly related to PCD mineralization. Data classification was rigorously validated by cross-referencing age, geological context, spatial distribution, and tectonic environment to ensure accurate assignment of PCDs to either subduction or collision zones. The dataset includes 24 PCDs from subduction zones and 20 from collision zones (Fig. 1). We aimed to compile the most complete datasets available while ensuring a balanced representation between the two tectonic settings.

Apatite, amphibole, and zircon data were obtained from ore-forming magmas contemporaneous with mineralization. To ensure representativeness, we selected amphibole phenocrysts, as they record critical information about the evolution of magmas in crustal reservoirs. Non-primary amphibole data, such as those exhibiting deformation features or identified as xenocrysts, were excluded. For apatite, we focused on magmatic apatite, primarily derived from crystals enclosed within fresh or minimally altered magmatic minerals, such as amphibole, biotite, and zircon. This approach minimizes the influence of hydrothermal alteration on the dataset [34, 51]. Additionally, selected apatite crystals exhibited euhedral morphologies and showed no signs of alteration in cathodoluminescence or backscattered electron images.

7.2 Whole-Rock Geochemical Modeling

We employed the Monte Carlo method to simulate petrological processes, constraining the behavior of PGEs and metal components (e.g., Cu) in ore-forming magmas during magma evolution driven by sulfide and fluid saturation. Using mass balance and petrological modeling approaches, we randomly determined pressure and temporal parameters of the magmatic system, generating corresponding residual melt characteristics [47]. The modeled pressure range was set between 0.5 and 5 kbar, representing crustal magmatic evolution conditions and consistent with pressure estimates from amphibole barometry (Extended Data Fig. 6). The time range was set from 0 to 7 Ma to enable residual melt parameterization [41]. Based on experimental petrology results [52–54], polynomial fitting was performed to establish the relationships between MgO, FeO_T, and temperature (T) versus the degree of crystallization, enabling the determination of residual melt compositional characteristics:

$$C_{\text{MgO}}^{\text{SM}} = 0.00087702 \times (X^{\text{Total}})^2 - 0.18263 \times X^{\text{Total}} + 9.4607 \quad (R^2 = 0.97) \quad (1)$$

$$C_{\text{FeOt}}^{\text{SM}} = 0.017063 \times (C_{\text{MgO}}^{\text{SM}})^3 - 0.37395 \times (C_{\text{MgO}}^{\text{SM}})^2 + 2.8962 \times C_{\text{MgO}}^{\text{SM}} - 0.16721 \quad (R^2 = 0.94) \quad (2)$$

$$T = 871.09 \times C_{\text{MgO}}^{\text{SM}^{1.1289}} \quad (R^2 = 0.96) \quad (3)$$

$C_{\text{MgO}}^{\text{SM}}$ and $C_{\text{FeOt}}^{\text{SM}}$ represent the MgO and FeOt content of the residual magma (in wt%). X^{Total} is the total magma crystallinity. There remain multiple perspectives on the source regions and mechanisms responsible for generating the ore-forming juvenile magmas in subduction and collision zones [5, 7, 8, 16, 17]. To simplify the models and enable a clearer comparison of differences in actual datasets, we adopted uniform parameter settings in our simulations.

Under sulfide-undersaturated conditions, sulfur is enriched in the residual silicate melt during magmatic differentiation. However, as magma evolves and its temperature decreases, the solubility of sulfur in the melt progressively declines, eventually leading to sulfide saturation. The original sulfur content is strongly dependent on oxygen fugacity ($f\text{O}_2$). Using data from primary melt inclusions [55], we derived a quantitative relationship between original sulfur content and $f\text{O}_2$ through polynomial fitting. The $f\text{O}_2$ range was constrained between ΔFMQ 0 and +3.5, allowing us to determine the corresponding original sulfur content characteristics. The relevant equation is as follows:

$$\Delta\text{FMQ} = 0.51071 \times \ln(C_{\text{Sulfur}}^{\text{O}}) + 1.8171 \quad (R^2 = 0.73) \quad (4)$$

$C_{\text{Sulfur}}^{\text{O}}$ is sulfur concentration in the original melt. The solubility of sulfur is controlled by melt temperature, pressure, $f\text{O}_2$, and MgO content [56–58]. We assumed that sulfur precipitates exclusively as sulfide upon saturation, with the sulfur content in sulfides set to 36.5 wt%. Based on the discussions presented earlier in this study and relevant literature, the distribution of Cu, Pd, and Pt into minerals other than sulfides was neglected [59, 60]. The partition coefficient of Cu between sulfides and silicate melt, which is significantly influenced by $f\text{O}_2$, temperature, and MgO content, was calculated using the model of parameters mentioned above [61]. The partition coefficient of Pd is slightly higher than that of Pt, with values set in the ranges of 480 to 35000 [62, 63] and 20 to 8700 [64], respectively.

As magma evolves, the solubility of water in the melt progressively decreases until fluid saturation is reached. As discussed in the text, the exsolved fluid phase significantly enriches Cu and Pt. We set the initial water content between 2 and 8 wt%.

Based on the experimental calibration by Tattitch and Blundy [65], the fluid–melt partition coefficient for Cu can be determined as a function of NaCl, water, and H₂S concentrations in the fluid. For simplicity, the fluid H₂S content is assumed to be zero. The NaCl content of the fluid is constrained by the Cl partitioning behavior between the fluid and melt, which is governed by the Cl concentration in the melt, the melt SiO₂ content, and the system pressure [66]. Melt Cl concentrations are set between 0.2 and 0.6 wt%, and the fluid–melt Cl partition coefficient is calculated accordingly. These parameters are then used to derive the Cu partition coefficient between fluid and melt. The partition coefficients of Pt and Pd between fluid and silicate melt are set in the range of 100–10,000 for Pt and 0.1–1,000 for Pd, with Pt generally exhibiting higher fluid–melt compatibility than Pd [67–70]. The initial concentrations of Cu, Pd, and Pt were set at 40–90 ppm [71], 1–10 ppb [24, 72] and 1.5–5 ppb [23], respectively. Considering that this study simulates the evolution of magma in crustal magma chambers, we adopted an ideal equilibrium crystallization model [73].

7.3 Evolution of Melt Volatiles Under Fluid-Saturated and Undersaturated Conditions

We calculated the apatite–melt volatile partition coefficients based on temperature and regression experimental data, using Gibbs free energy and exchange parameters to determine melt volatile ratios from apatite compositions [35]. This approach eliminates reliance on empirical partition coefficients, instead calculating volatile partition coefficients individually for each apatite sample. The AST, derived from whole-rock compositions, was used to represent the crystallization temperature of apatite. To simulate the volatile ratios of ore-forming melts in subduction and collision zones, we employed Monte Carlo modeling [36] to compare degassing efficiencies between the two tectonic settings. Given that apatite crystallizes relatively late in magmatic systems [36, 74], the model focuses solely on “second boiling” processes associated with crystallization [36]. To account for uncertainties in initial conditions, parameters were randomly selected from predefined reasonable ranges. The pressure range was set between 1.6 and 3.0 kbar, corresponding to the pressures relevant to shallow magmatic evolution processes in magma chambers. Water solubility was constrained as a function of pressure using a linear regression model [36, 46].

In the fluid-saturated model, the Cl content of the melt was set between 0.2 and 0.6 wt%, while the F content ranged from 0.04 to 0.18 wt%, both considered reasonable and broad ranges [75, 76]. The model assumes an initial melt volume of 100%, which gradually cools and crystallizes in 1% increments along the liquid line of descent. Due to the sensitivity of this process to temperature variations associated with fluid exsolution, we fitted magmatic evolution experimental data focused on fluid degassing [54] using a second-order polynomial regression, establishing the relationship between temperature, melt SiO₂ content, and crystallization degree [36]. In the fluid-undersaturated model, SiO₂ content and temperature of the melt were not input parameters [36].

The fluid–melt partition coefficient of Cl is controlled by melt Cl content, SiO₂ content, and pressure, and was determined using experimentally calibrated equations [36, 66]. Since the fluid–melt partition behavior of F remains incompletely understood,

existing experiments suggest that F preferentially remains in the melt under shallow crustal pressure conditions [77, 78]. To accommodate potential variability, the partition coefficient of F was set between 0.01 and 1.

7.4 Modeling the Correlation Between Initial Water Content and Magma Emplacement Depth

We performed systematic simulations of melt properties, including density and viscosity, during magma ascent and degassing using rhyolite-MELTS 1.2.0 [46]. The model used the starting compositions from magmatic evolution experiments related to fluid exsolution [54]. The initial CO₂ content was set to 5000 ppm [79], while the initial water content ranged from 2 to 8 wt%.

Magma ascent was modeled as an adiabatic process, starting at an initial pressure of 10 kbar and proceeding in decompression steps of 0.1 kbar. Both open- and closed-system crystallization and volatile saturation behaviors were considered [43]. The simulated results and pressures estimated from amphibole barometry were converted into storage depths using density models of convergent plate boundaries [43]. The viscosity knee on the viscosity-pressure curve was calculated using the algorithm from the Knead Python package [80]. To avoid errors caused by minor "turning points" along the curve, the sensitivity parameter (S) was set to a relatively high value (10), ensuring the reliability of the fitting results [43].

Declarations

- Acknowledgements: We express our gratitude to Siqi Liu, Yang Shen, and Changda Wu for their valuable discussions. This project was funded by the National Natural Science Foundation of China (Grant Nos. U2344204, 42202081), the National Key Research and Development Program of China (Grant No. 2019YFA0708602), and Frontiers Science Center for Deep-Time Digital Earth (Grant No. 2652023001).
- Competing interests: The authors declare no competing financial interests.
- Ethics approval and consent to participate: Not applicable
- Consent for publication: Not applicable
- Data availability: The authors declare that all data that were generated in this study are provided in the files Supplementary Table S1–4. Source data are provided with this paper.
- Materials availability: Not applicable
- Code availability: The Python code used to perform the Monte Carlo simulations is available at
- Author contribution: Y.C.Z. and Z.X.W. designed the project. Z.X.W. compiled and organized the dataset and conducted the Monte Carlo and geochemical simulations. Z.X.W. and Y.C.Z. wrote the manuscript. All authors contributed to the interpretation of the results and the preparation of the manuscript.

References

- [1] Edmonds, M., Mason, E., Hogg, O.: Volcanic outgassing of volatile trace metals.

- [2] Nathwani, C., Blundy, J., Large, S.J., Wilkinson, J.J., Buret, Y., Loader, M.A., Tavazzani, L., Chelle-Michou, C.: A zircon case for super-wet arc magmas. *Nature Communications* **15**(1), 8982 (2024)
- [3] Rezeau, H., Jagoutz, O.: The importance of h₂o in arc magmas for the formation of porphyry cu deposits. *Ore Geology Reviews* **126**, 103744 (2020)
- [4] Sillitoe, R.H.: A plate tectonic model for the origin of porphyry copper deposits. *Economic geology* **67**(2), 184–197 (1972)
- [5] Wilkinson, J.J.: Triggers for the formation of porphyry ore deposits in magmatic arcs. *Nature Geoscience* **6**(11), 917–925 (2013)
- [6] Wang, Z., Zheng, Y., Xu, B., Hou, Z., Shen, Y., Zhang, A., Wang, L., Wu, C., Guo, Q.: Mechanisms of fluid degassing in shallow magma chambers control the formation of porphyry deposits. *American Mineralogist* **109**(12), 2073–2085 (2024)
- [7] Lamont, T.N., Loader, M.A., Roberts, N.M., Cooper, F.J., Wilkinson, J.J., Bevan, D., Gorecki, A., Kemp, A., Elliott, T., Gardiner, N.J., et al.: Porphyry copper formation driven by water-fluxed crustal melting during flat-slab subduction. *Nature Geoscience*, 1–10 (2024)
- [8] Hou, Z., Yang, Z., Lu, Y., Kemp, A., Zheng, Y., Li, Q., Tang, J., Yang, Z., Duan, L.: A genetic linkage between subduction-and collision-related porphyry cu deposits in continental collision zones. *Geology* **43**(3), 247–250 (2015)
- [9] Ducea, M.N., Paterson, S.R., DeCelles, P.G.: High-volume magmatic events in subduction systems. *Elements* **11**(2), 99–104 (2015)
- [10] Richards, J.P.: A shake-up in the porphyry world? *Economic Geology* **113**(6), 1225–1233 (2018)
- [11] Cawood, P.A., Kröner, A., Collins, W.J., Kusky, T.M., Mooney, W.D., Windley, B.F.: Accretionary orogens through earth history. In: *Earth Accretionary Systems in Space and Time*. Geological Society of London, ??? (2009). <https://doi.org/10.1144/SP318.1> . <https://doi.org/10.1144/SP318.1>
- [12] Xiao, W., Han, C., Yuan, C., Sun, M., Zhao, G., Shan, Y.: Transitions among mariana-, japan-, cordillera- and alaska-type arc systems and their final juxtapositions leading to accretionary and collisional orogenesis. In: *The Evolving Continents: Understanding Processes of Continental Growth*. Geological Society of London, ??? (2010). <https://doi.org/10.1144/SP338.3> . <https://doi.org/10.1144/SP338.3>

- [13] Zhu, D.-C., Wang, Q., Weinberg, R.F., Cawood, P.A., Chung, S.-L., Zheng, Y.-F., Zhao, Z., Hou, Z.-Q., Mo, X.-X.: Interplay between oceanic subduction and continental collision in building continental crust. *Nature Communications* **13**(1), 7141 (2022)
- [14] FYFE, W.: Subduction and the structure of andesitic volcanic belts. *Am. J. Sci.* **275**, 285–297 (1975)
- [15] Grove, T.L., Till, C.B., Krawczynski, M.J.: The role of h₂o in subduction zone magmatism. *Annual Review of Earth and Planetary Sciences* **40**(1), 413–439 (2012)
- [16] Chang, J., Audétat, A.: Post-subduction porphyry cu magmas in the sanjiang region of southwestern china formed by fractionation of lithospheric mantle-derived mafic magmas. *Geology* **51**(1), 64–68 (2023)
- [17] Yang, Z., Cao, K.: Post-collisional porphyry copper deposits in tibet: An overview. *Earth-Science Reviews*, 104954 (2024)
- [18] Lu, Y.-J., Kerrich, R., Kemp, A.I., McCuaig, T.C., Hou, Z.-Q., Hart, C.J., Li, Z.-X., Cawood, P.A., Bagas, L., Yang, Z.-M., *et al.*: Intracontinental eocene-oligocene porphyry cu mineral systems of yunnan, western yangtze craton, china: compositional characteristics, sources, and implications for continental collision metallogeny. *Economic Geology* **108**(7), 1541–1576 (2013)
- [19] Hou, Z., Wang, R., Zhang, H., Zheng, Y., Jin, S., Thybo, H., Weinberg, R.F., Xu, B., Yang, Z., Hao, A.-W., *et al.*: Formation of giant copper deposits in tibet driven by tearing of the subducted indian plate. *Earth-Science Reviews* **243**, 104482 (2023)
- [20] Richards, J.: Tectono-magmatic precursors for porphyry cu-(mo-au) deposit formation. *Economic geology* **98**(8), 1515–1533 (2003)
- [21] Campbell, I.H., Stepanov, A.S., Liang, H.-Y., Allen, C.M., Norman, M.D., Zhang, Y.-Q., Xie, Y.-W.: The origin of shoshonites: new insights from the tertiary high-potassium intrusions of eastern tibet. *Contributions to Mineralogy and Petrology* **167**, 1–22 (2014)
- [22] Weller, O.M., Mottram, C.M., St-Onge, M.R., Möller, C., Strachan, R., Rivers, T., Copley, A.: The metamorphic and magmatic record of collisional orogens. *Nature Reviews Earth & Environment* **2**(11), 781–799 (2021)
- [23] Woodland, S., Pearson, D., Thirlwall, M.: A platinum group element and re-os isotope investigation of siderophile element recycling in subduction zones: comparison of grenada, lesser antilles arc, and the izu-bonin arc. *Journal of Petrology* **43**(1), 171–198 (2002)

- [24] Park, J.-W., Campbell, I.H., Kim, J., Moon, J.-W.: The role of late sulfide saturation in the formation of a cu-and au-rich magma: insights from the platinum group element geochemistry of niuatahi-motutahi lavas, tonga rear arc. *Journal of Petrology* **56**(1), 59–81 (2015)
- [25] Park, J.-W., Campbell, I.H., Malaviarachchi, S.P., Cocker, H., Hao, H., Kay, S.M.: Chalcophile element fertility and the formation of porphyry cu±au deposits. *Mineralium Deposita* **54**, 657–670 (2019)
- [26] Core, D.P., Kesler, S.E., Essene, E.J.: Unusually cu-rich magmas associated with giant porphyry copper deposits: Evidence from bingham, utah. *Geology* **34**(1), 41–44 (2006)
- [27] Chiaradia, M., Caricchi, L.: Stochastic modelling of deep magmatic controls on porphyry copper deposit endowment. *Scientific reports* **7**(1), 44523 (2017)
- [28] Du, J., Audétat, A.: Early sulfide saturation is not detrimental to porphyry cu-au formation. *Geology* **48**(5), 519–524 (2020)
- [29] Chiaradia, M., Caricchi, L.: Supergiant porphyry copper deposits are failed large eruptions. *Communications Earth & Environment* **3**(1), 107 (2022)
- [30] Park, J.-W., Campbell, I.H., Kim, J.: Abundances of platinum group elements in native sulfur condensates from the niuatahi-motutahi submarine volcano, tonga rear arc: implications for pge mineralization in porphyry deposits. *Geochimica et Cosmochimica Acta* **174**, 236–246 (2016)
- [31] Hao, H., Campbell, I.H., Park, J.-W., Cooke, D.R.: Platinum-group element geochemistry used to determine cu and au fertility in the northparkes igneous suites, new south wales, australia. *Geochimica et Cosmochimica Acta* **216**, 372–392 (2017)
- [32] Piccoli, P.M., Candela, P.A.: Apatite in igneous systems. *Reviews in Mineralogy and Geochemistry* **48**(1), 255–292 (2002)
- [33] Stock, M.J., Humphreys, M.C., Smith, V.C., Isaia, R., Pyle, D.M.: Late-stage volatile saturation as a potential trigger for explosive volcanic eruptions. *Nature Geoscience* **9**(3), 249–254 (2016)
- [34] Huang, M.-L., Zhu, J.-J., Chiaradia, M., Hu, R.-Z., Xu, L.-L., Bi, X.-W.: Apatite volatile contents of porphyry cu deposits controlled by depth-related fluid exsolution processes. *Economic Geology* **118**(5), 1201–1217 (2023)
- [35] Li, W., Costa, F.: A thermodynamic model for f-cl-oh partitioning between silicate melts and apatite including non-ideal mixing with application to constraining melt volatile budgets. *Geochimica et Cosmochimica Acta* **269**, 203–222 (2020)

- [36] Nathwani, C.L., Large, S.J., Brugge, E.R., Wilkinson, J.J., Buret, Y., EIMF: Apatite evidence for a fluid-saturated, crystal-rich magma reservoir forming the quellaveco porphyry copper deposit (southern peru). *Contributions to Mineralogy and Petrology* **178**(8), 49 (2023)
- [37] Chiaradia, M.: How much water in basaltic melts parental to porphyry copper deposits? *Frontiers in Earth Science* **8**, 138 (2020)
- [38] Moore, G.: Interpreting h₂o and co₂ contents in melt inclusions: constraints from solubility experiments and modeling. *Reviews in Mineralogy and Geochemistry* **69**(1), 333–362 (2008)
- [39] Chelle-Michou, C., Chiaradia, M., Beguelin, P., Ulianov, A.: Petrological evolution of the magmatic suite associated with the corocohuayco cu (–au–fe) porphyry–skarn deposit, peru. *Journal of Petrology* **56**(9), 1829–1862 (2015)
- [40] Leshner, C.E., Spera, F.J.: Thermodynamic and transport properties of silicate melts and magma. In: *The Encyclopedia of Volcanoes*, pp. 113–141. Elsevier, ??? (2015)
- [41] Annen, C., Blundy, J., Sparks, R.: The genesis of intermediate and silicic magmas in deep crustal hot zones. *Journal of Petrology* **47**(3), 505–539 (2006)
- [42] Keller, C.B., Schoene, B., Barboni, M., Samperton, K.M., Husson, J.M.: Volcanic–plutonic parity and the differentiation of the continental crust. *Nature* **523**(7560), 301–307 (2015)
- [43] Rasmussen, D.J., Plank, T.A., Roman, D.C., Zimmer, M.M.: Magmatic water content controls the pre-eruptive depth of arc magmas. *Science* **375**(6585), 1169–1172 (2022)
- [44] Blundy, J., Cashman, K.: Ascent-driven crystallisation of dacite magmas at mount st helens, 1980–1986. *Contributions to Mineralogy and Petrology* **140**, 631–650 (2001)
- [45] Huber, C., Townsend, M., Degruyter, W., Bachmann, O.: Optimal depth of subvolcanic magma chamber growth controlled by volatiles and crust rheology. *Nature Geoscience* **12**(9), 762–768 (2019)
- [46] Ghiorso, M.S., Gualda, G.A.: An h₂o–co₂ mixed fluid saturation model compatible with rhyolite-melts. *Contributions to Mineralogy and Petrology* **169**, 1–30 (2015)
- [47] Chiaradia, M.: Gold endowments of porphyry deposits controlled by precipitation efficiency. *Nature Communications* **11**(1), 248 (2020)
- [48] Cooke, D.R., Hollings, P., Walshe, J.L.: Giant porphyry deposits: characteristics,

- distribution, and tectonic controls. *Economic geology* **100**(5), 801–818 (2005)
- [49] Marshak, S.: *Essentials of Geology*. WW Norton, ??? (2004)
 - [50] Chiaradia, M.: Distinct magma evolution processes control the formation of porphyry cu–au deposits in thin and thick arcs. *Earth and Planetary Science Letters* **599**, 117864 (2022)
 - [51] Kendall-Langley, L.A., Kemp, A.I., Hawkesworth, C.J., Hinton, E.J.C.C.T.R., Roberts, M.P.: Quantifying f and cl concentrations in granitic melts from apatite inclusions in zircon. *Contributions to Mineralogy and Petrology* **176**, 1–19 (2021)
 - [52] Nandedkar, R.H., Ulmer, P., Müntener, O.: Fractional crystallization of primitive, hydrous arc magmas: an experimental study at 0.7 gpa. *Contributions to Mineralogy and Petrology* **167**(6), 1015 (2014)
 - [53] Ulmer, P., Kaegi, R., Müntener, O.: Experimentally derived intermediate to silica-rich arc magmas by fractional and equilibrium crystallization at 1· 0 gpa: an evaluation of phase relationships, compositions, liquid lines of descent and oxygen fugacity. *Journal of Petrology* **59**(1), 11–58 (2018)
 - [54] Caricchi, L., Blundy, J.: Experimental petrology of monotonous intermediate magmas. Geological Society, London, Special Publications **422**(1), 105–130 (2015)
 - [55] Muth, M.J., Wallace, P.J.: Sulfur recycling in subduction zones and the oxygen fugacity of mafic arc magmas. *Earth and Planetary Science Letters* **599**, 117836 (2022)
 - [56] Mavrogenes, J.A., O'Neill, H.S.C.: The relative effects of pressure, temperature and oxygen fugacity on the solubility of sulfide in mafic magmas. *Geochimica et Cosmochimica Acta* **63**(7-8), 1173–1180 (1999)
 - [57] O'NEILL, H.S.C., Mavrogenes, J.A.: The sulfide capacity and the sulfur content at sulfide saturation of silicate melts at 1400 c and 1 bar. *Journal of Petrology* **43**(6), 1049–1087 (2002)
 - [58] Lee, C.-T.A., Luffi, P., Chin, E.J., Bouchet, R., Dasgupta, R., Morton, D.M., Le Roux, V., Yin, Q.-z., Jin, D.: Copper systematics in arc magmas and implications for crust-mantle differentiation. *Science* **336**(6077), 64–68 (2012)
 - [59] Liu, X., Xiong, X., Audétat, A., Li, Y.: Partitioning of cu between mafic minerals, fe–ti oxides and intermediate to felsic melts. *Geochimica et Cosmochimica Acta* **151**, 86–102 (2015)
 - [60] Chang, J., Audétat, A., Pettke, T.: The gold content of mafic to felsic potassic magmas. *Nature Communications* **15**(1), 6988 (2024)

- [61] Li, Y., Audétat, A.: Effects of temperature, silicate melt composition, and oxygen fugacity on the partitioning of v, mn, co, ni, cu, zn, as, mo, ag, sn, sb, w, au, pb, and bi between sulfide phases and silicate melt. *Geochimica et Cosmochimica Acta* **162**, 25–45 (2015)
- [62] Mungall, J.E., Brenan, J.M.: Partitioning of platinum-group elements and au between sulfide liquid and basalt and the origins of mantle-crust fractionation of the chalcophile elements. *Geochimica et Cosmochimica Acta* **125**, 265–289 (2014)
- [63] Peach, C., Mathez, E., Keays, R.: Sulfide melt-silicate melt distribution coefficients for noble metals and other chalcophile elements as deduced from morb: Implications for partial melting. *Geochimica et Cosmochimica Acta* **54**(12), 3379–3389 (1990)
- [64] Liu, Z., Li, Y.: Experimental constraints on the behavior of pt and re in oxidized arc magmas. *Earth and Planetary Science Letters* **603**, 117986 (2023)
- [65] Tattitch, B.C., Blundy, J.D.: Cu-mo partitioning between felsic melts and saline-aqueous fluids as a function of x nacleq, f o₂, and f s₂. *American Mineralogist* **102**(10), 1987–2006 (2017)
- [66] Tattitch, B., Chelle-Michou, C., Blundy, J., Loucks, R.R.: Chemical feedbacks during magma degassing control chlorine partitioning and metal extraction in volcanic arcs. *Nature communications* **12**(1), 1774 (2021)
- [67] Simon, A.C., Pettke, T.: Platinum solubility and partitioning in a felsic melt–vapor–brine assemblage. *Geochimica et Cosmochimica Acta* **73**(2), 438–454 (2009)
- [68] Sullivan, N.A., Zajacz, Z., Brenan, J.M., Hinde, J.C., Tsay, A., Yin, Y.: The solubility of gold and palladium in magmatic brines: Implications for pge enrichment in mafic-ultramafic and porphyry environments. *Geochimica et Cosmochimica Acta* **316**, 230–252 (2022)
- [69] Hanley, J.J., Pettke, T., Mungall, J.E., Spooner, E.T.: The solubility of platinum and gold in nacl brines at 1.5 kbar, 600 to 800 c: A laser ablation icp-ms pilot study of synthetic fluid inclusions. *Geochimica et Cosmochimica Acta* **69**(10), 2593–2611 (2005)
- [70] Sullivan, N.A., Zajacz, Z., Brenan, J.M., Tsay, A.: The solubility of platinum in magmatic brines: Insights into the mobility of pge in ore-forming environments. *Geochimica et Cosmochimica Acta* **316**, 253–272 (2022)
- [71] Chiaradia, M.: Copper enrichment in arc magmas controlled by overriding plate thickness. *Nature Geoscience* **7**(1), 43–46 (2014)
- [72] Park, J.-W., Campbell, I.H., Eggins, S.M.: Enrichment of rh, ru, ir and os in

- cr spinels from oxidized magmas: Evidence from the ambae volcano, vanuatu. *Geochimica et Cosmochimica Acta* **78**, 28–50 (2012)
- [73] Rollinson, H.R.: *Using Geochemical Data: Evaluation, Presentation, Interpretation*. Routledge, ??? (2014)
- [74] Miles, A., Graham, C., Hawkesworth, C., Gillespie, M., Hinton, R., uk, E.I.M.F.E.: Evidence for distinct stages of magma history recorded by the compositions of accessory apatite and zircon. *Contributions to Mineralogy and Petrology* **166**, 1–19 (2013)
- [75] Aiuppa, A., Baker, D., Webster, J.: Halogens in volcanic systems. *Chemical Geology* **263**(1-4), 1–18 (2009)
- [76] Webster, J.D., Baker, D.R., Aiuppa, A.: Halogens in mafic and intermediate-silica content magmas. The role of halogens in terrestrial and extraterrestrial geochemical processes: surface, crust, and mantle, 307–430 (2018)
- [77] Webster, J.D., Holloway, J.R.: Partitioning of f and cl between magmatic hydrothermal fluids and highly evolved granitic magmas. In: *Ore-bearing Granite Systems; Petrogenesis and Mineralizing Processes*. Geological Society of America, ??? (1990)
- [78] Cassidy, M., Iveson, A.A., Humphreys, M.C., Mather, T.A., Helo, C., Castro, J.M., Ruprecht, P., Pyle, D.M., EIMF: Experimentally derived f, cl, and br fluid/melt partitioning of intermediate to silicic melts in shallow magmatic systems. *American Mineralogist* **107**(10), 1825–1839 (2022)
- [79] Mironov, N., Portnyagin, M., Botcharnikov, R., Gurenko, A., Hoernle, K., Holtz, F.: Quantification of the co₂ budget and h₂o–co₂ systematics in subduction-zone magmas through the experimental hydration of melt inclusions in olivine at high h₂o pressure. *Earth and Planetary Science Letters* **425**, 1–11 (2015)
- [80] Satopaa, V., Albrecht, J., Irwin, D., Raghavan, B.: 2011 31st international conference on distributed computing systems workshops. IEEE Manhattan, NY (2011)



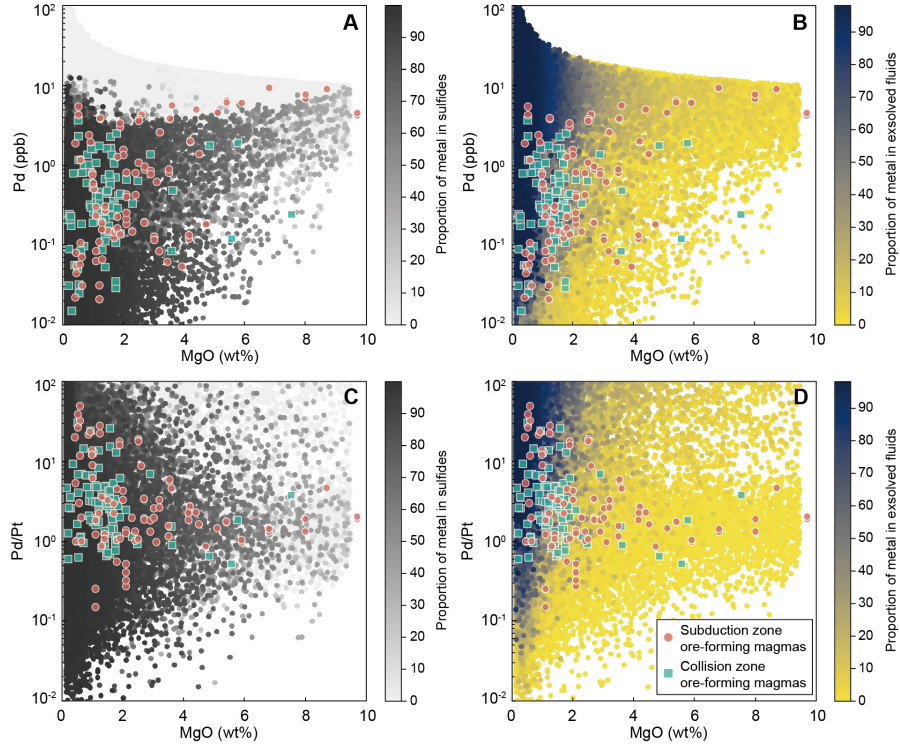


Fig. 2 Comparison and Models of Pd Composition and Pd/Pt Ratios in Subduction and Collision Zone Ore-Forming Magmas. a, b, Pd content vs MgO content. c, d, with a total of 100000 simulations conducted to evaluate the effects of magma processes on Pd and Pd/Pt distributions. The color bars indicate the proportion of metals in sulfide or exsolved fluids during the simulations, highlighting the effects of sulfide saturation and degassing processes. Refer to Methods for details of the modelling.

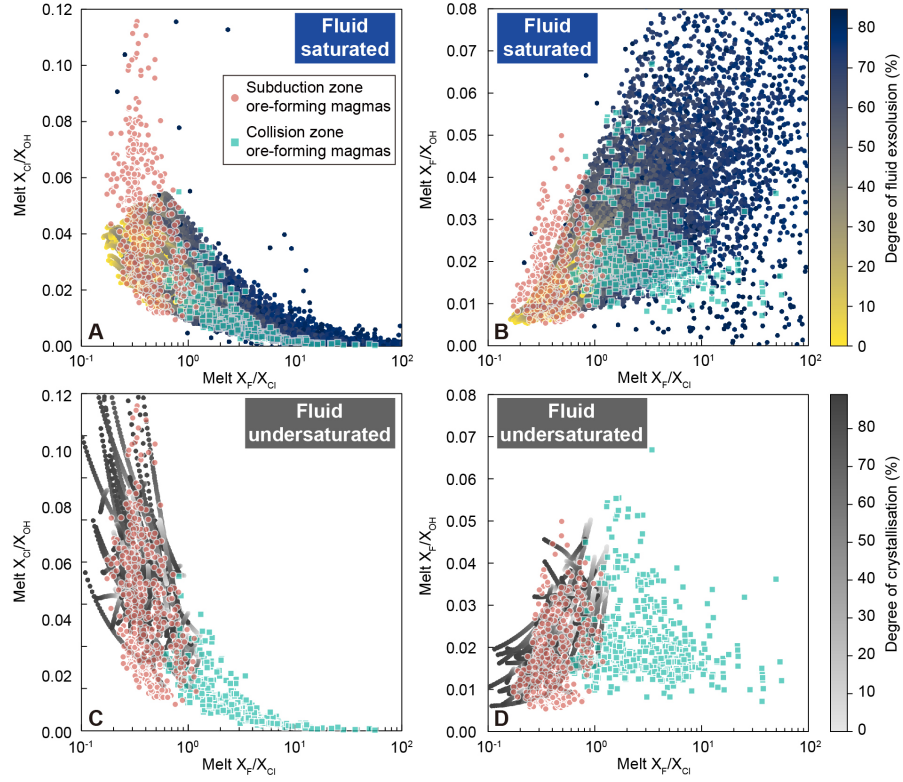


Fig. 3 Comparison and Models of Volatile Ratios in Subduction and Collision Zone Ore-Forming Magmas. **a, b,** X_{Cl}/X_{OH} vs. X_F/X_{OH} and X_{Cl}/X_{OH} vs. X_F/X_{Cl} for fluid-saturated magma evolving as a function of melt crystallisation. **c, d,** model results for fluid-undersaturated magma evolving. Symbols represent melt compositions for subduction and collision zone ore-forming magmas calculated from apatite. The color bars denote the degree of fluid exsolution (**a, b**) or degree of crystallisation (**c, d**).

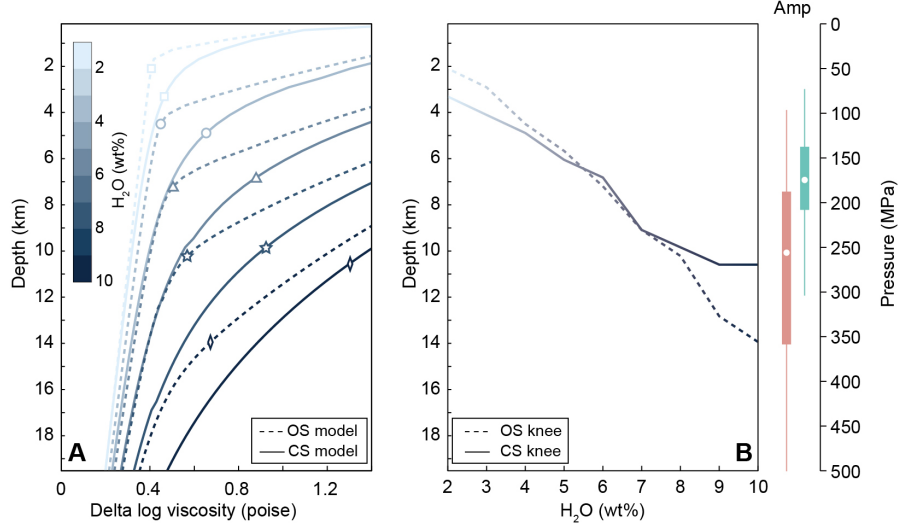


Fig. 4 Relationship Between Magma Water Content, Viscosity, and Emplacement Depth. **a**, Viscosity evolution of juvenile magmas with varying water contents (shading transitions from light to dark blue, representing 2, 4, 6, and 8 wt% water contents) during adiabatic ascent, modeled using rhyolite-MELTS [46]. The model considers crystallization and volatile exsolution processes under both open- and closed-system conditions. Different markers indicate the viscosity knee points corresponding to varying water contents. Additional modeling details are provided in the Methods. **b**, Depths corresponding to the viscosity knees of juvenile magmas with different water contents under open- and closed-system conditions. On the right, melt storage pressures derived from amphibole compositions are shown. The teal box represents pressures for collision zone ore-forming magmas, indicating relatively shallower storage depths. In contrast, the pink box corresponds to subduction zone ore-forming magmas, reflecting deeper magma emplacement depths. The boxes represent the interquartile range (IQR, 25th to 75th percentiles), with the central white circles showing the median values. The whiskers extend to the maximum and minimum values within 1.5 times the IQR.

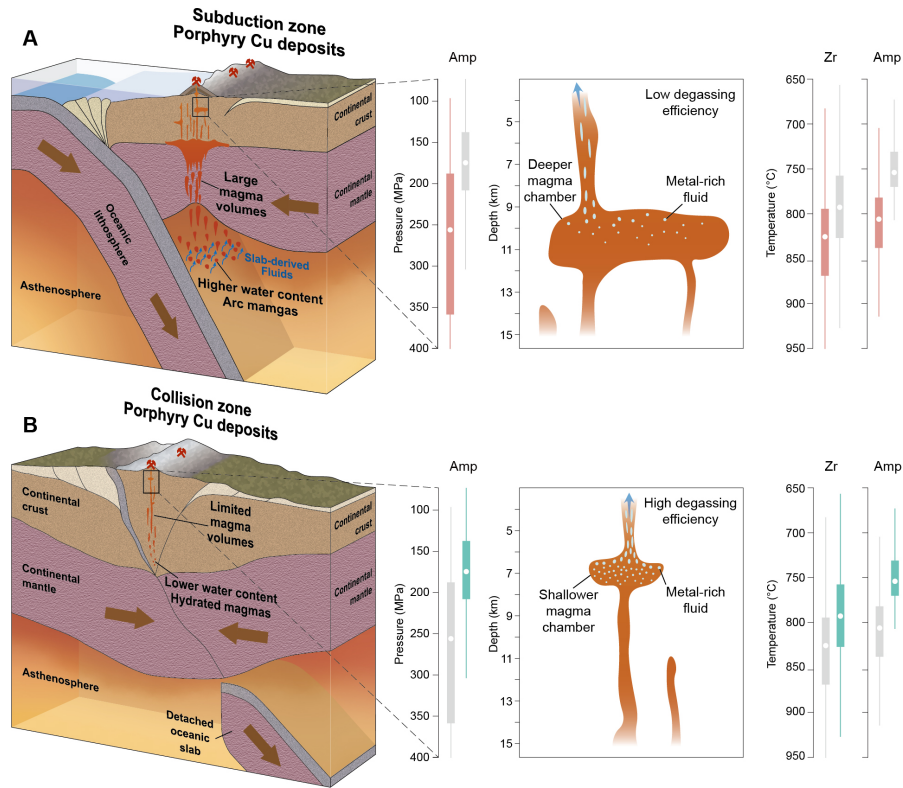
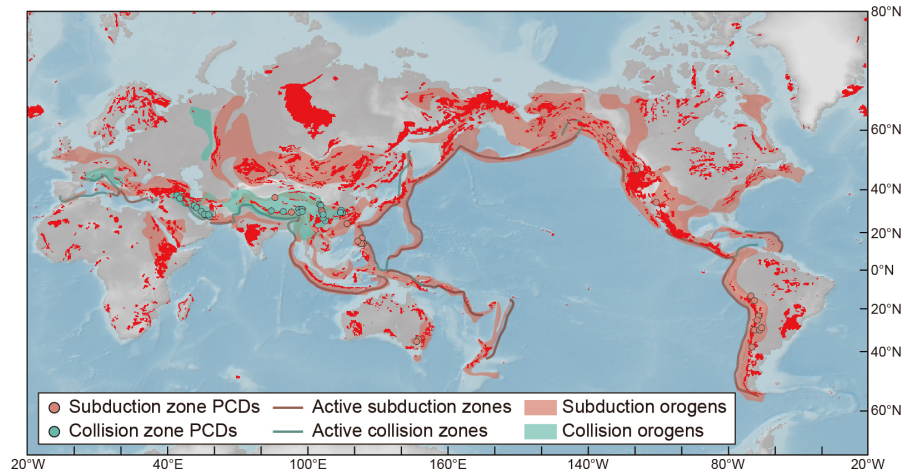
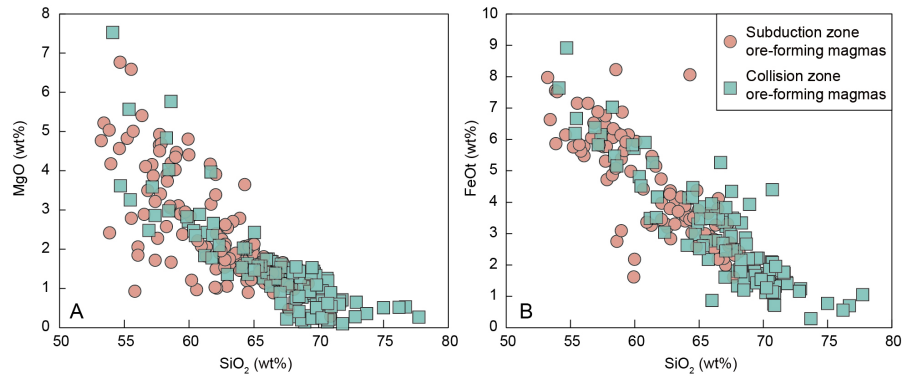


Fig. 5 The Distinct Synergistic Frameworks of Magmatic Properties, Structure, and Volume for Porphyry Cu Deposits in Subduction and Collision Zones. **a**, In subduction zones, volatiles directly supplied by the subduction of oceanic slabs result in higher initial water contents of ore-forming magmas. This promotes the formation of deeper magma reservoirs, thereby reducing degassing efficiency. However, large magma volumes in subduction zones compensate for the low degassing efficiencies, enabling sufficient fluids to exsolve. These fluids transport large amounts of ore-forming materials, which migrate and accumulate in the upper crust, ultimately forming PCDs. **b**, In collision zones, ore-forming magmas are characterized by significantly lower magma volumes. Due to the absence of oceanic slab subduction as a volatile source, the initial water contents of ore-forming magmas in collision zones are relatively low. This lower water content leads to the formation of shallower magma reservoirs, enhancing degassing efficiency. Efficient degassing processes allow even magmas with low volumes to exsolve large-scale magmatic fluids capable of transporting substantial ore-forming materials, resulting in PCD mineralization. The conceptual model is referenced from Marshak 2004 [49]. The box-and-whisker plot follows the same definition as in Fig. 4.

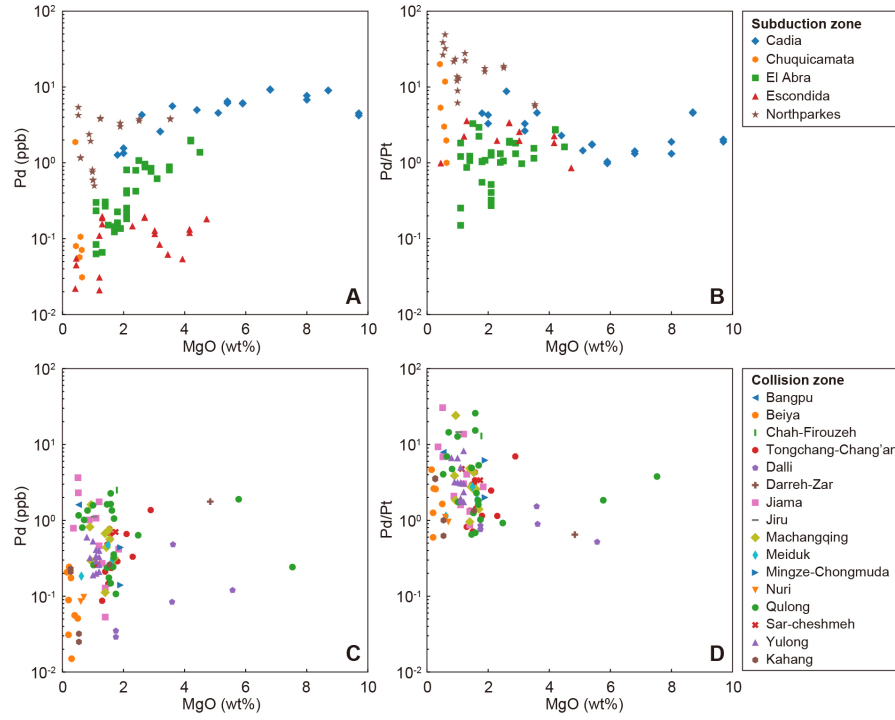
Extended Data



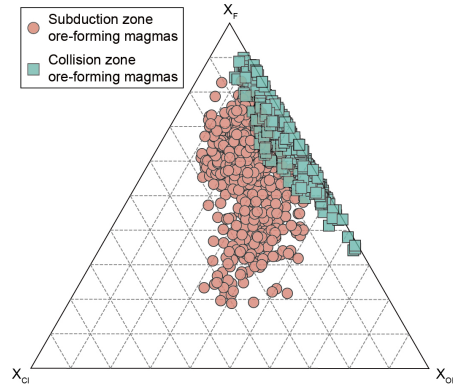
Extended Data Fig. 1 Global Distribution of Igneous Rocks. The map illustrates the global distribution of igneous rocks derived from the Macrostrat database (<https://macrostrat.org>), based on a 1:20,000,000-scale dataset. Additionally, the figure highlights the distribution of orogenic belts associated with subduction and collisional processes. The locations of porphyry Cu deposits investigated in this study within relevant subduction and collision zones are also marked.



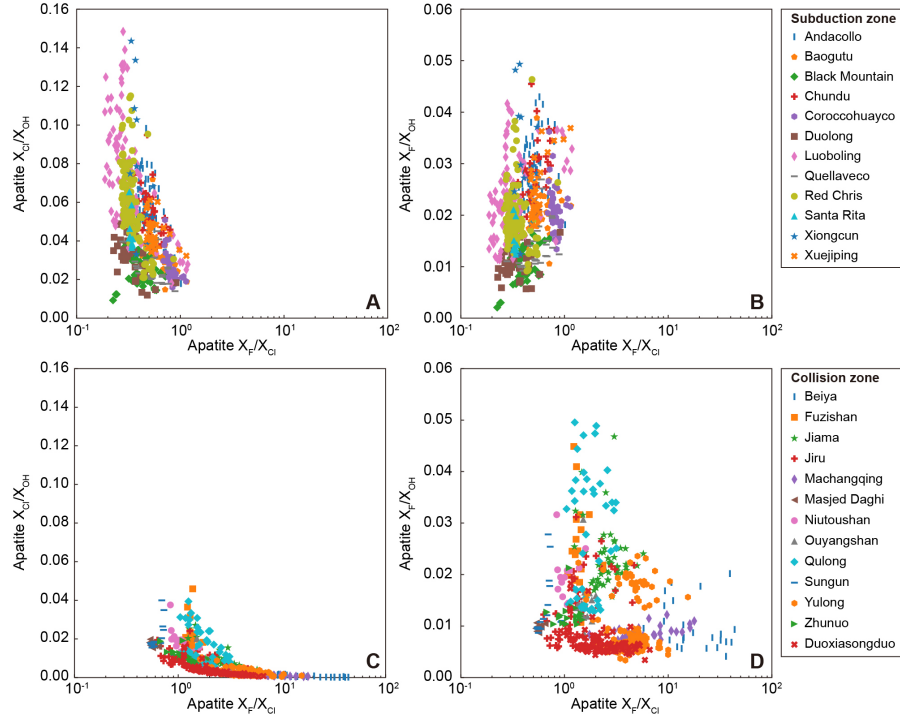
Extended Data Fig. 2 Whole-Rock Major Element Characteristics of Ore-Forming Magmas in Subduction and Collision Zones. a, b, MgO vs. SiO₂ contents (a) and FeOt vs. SiO₂ contents (b) diagrams for ore-forming magmas in subduction and collision zones.



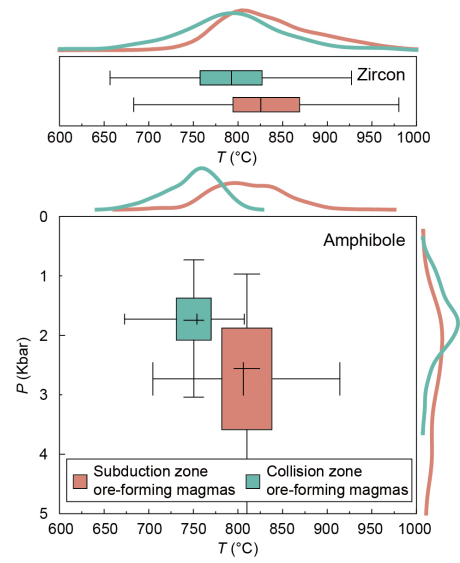
Extended Data Fig. 3 PGE features of Ore-Forming Magmas in Subduction and Collision Zones. a, b, Pd contents and Pd/Pt ratios vs. MgO contents of subduction zone ore-forming magmas. c, d, Pd contents and Pd/Pt ratios vs. MgO contents of collision zone ore-forming magmas. Symbols correspond to individual PCDs as indicated in the legend, emphasizing the contrasting trends between the two tectonic settings.



Extended Data Fig. 4 Ternary Space of Volatile Compositions of Apatites from Ore-Forming Magmas in Subduction and Collision Zones. Stark contrasts in volatile compositions are observed between apatites from subduction zone and collision zone ore-forming magmas. Apatites in subduction zones exhibit higher Cl and lower F contents, while those in collision zones are enriched in F and relatively depleted in Cl.



Extended Data Fig. 5 Volatile ratios of Apatites from Ore-Forming Magmas in Subduction and Collision Zones. a, b, Apatite X_F/X_{Cl} vs. X_{OH}/X_{Cl} and X_F/X_{Cl} vs. X_{OH}/X_F for subduction zone ore-forming magmas. c, d, Apatite X_F/X_{Cl} vs. X_{OH}/X_{Cl} and X_F/X_{Cl} vs. X_{OH}/X_F for collision zone ore-forming magmas. The data illustrate the contrasting volatile ratios in apatites between subduction and collision zones, reflecting systematic variations in apatite volatile compositions across these two tectonic settings. Different symbols correspond to various PCDs as shown in the legend.



Extended Data Fig. 6 Pressure and Temperature Conditions Calculated by Amphiboles and Zircons from Ore-forming Magmas in Collision and Subduction Zones. The box-and-whisker plot follows the same definition as in Fig. 4. The teal and pink lines represent the density of P and T